Structural Analysis of Adenine Phosphoribosyltransferase from *Saccharomyces cerevisiae*[†,‡]

Wuxian Shi,[⊥,#] Kelly S. E. Tanaka,[⊥,#] Timothy R. Crother,[§] Milton W. Taylor,[§] Steven C. Almo,[⊥] and Vern L. Schramm*[,⊥]

Department of Biochemistry, Albert Einstein College of Medicine, 1300 Morris Park Avenue, Bronx, New York 10461, and Department of Biology, Indiana University, Bloomington, Indiana 47405

Received March 7, 2001; Revised Manuscript Received July 9, 2001

ABSTRACT: Adenine phosphoribosyltransferase (APRTase) is a widely distributed enzyme, and its deficiency in humans causes the accumulation of 2,8-dihydroxyadenine. It is the sole catalyst for adenine recycling in most eukaryotes. The most commonly expressed APRTase has subunits of approximately 187 amino acids, but the only crystal structure is from *Leishmania donovani*, which expresses a long form of the enzyme with 237 residues. *Saccharomyces cerevisiae* APRTase was selected as a representative of the short APRTases, and the structure of the apo-enzyme and sulfate bound forms were solved to 1.5 and 1.75 Å, respectively. Yeast APRTase is a dimeric molecule, and each subunit is composed of a central five-stranded β-sheet surrounded by five α-helices, a structural theme found in all known purine phosphoribosyltransferases. The structures reveal several important features of APRTase function: (i) sulfate ions bound at the 5′-phosphate and pyrophosphate binding sites; (ii) a nonproline cis peptide bond (Glu67−Ser68) at the pyrophosphate binding site in both apo-enzyme and sulfate-bound forms; and (iii) a catalytic loop that is open and ordered in the apo-enzyme but open and disordered in the sulfate-bound form. Alignment of conserved amino acids in short-APRTases from 33 species reveals 13 invariant and 15 highly conserved residues present in hinges, catalytic site loops, and the catalytic pocket. Mutagenesis of conserved residues in the catalytic loop, subunit interface, and phosphoribosylpyrophosphate binding site indicates critical roles for the tip of the catalytic loop (Glu106) and a catalytic site residue Arg69, respectively. Mutation of one loop residue (Tyr103Phe) increases k_{cat} by 4-fold, implicating altered dynamics for the catalytic site loop.

Adenine phosphoribosyltransferase (APRTase)[1] catalyzes the reversible formation of AMP and pyrophosphate from adenine and 5-phospho-α-D-ribosyl-1-pyrophosphate (PRPP) in the presence of Mg^{2+} (Figure 1a) (*1*). The primary role of APRTases is salvage or recycling of adenine to re-form adenine nucleotides (*2*−*6*). In mammals, adenine is formed only in the pathway of polyamine synthesis from *S*-adenosylmethionine and is salvaged to the adenine nucleotide pool only by APRTase (Figure 1b).

APRTase is also present in purine auxotrophs, including the protozoan parasites. It is competent for purine uptake based on the observation that adenine can satisfy the requirement for exogenous purines in these organisms (*5*). However, genetic deletion of APRTase in *Leishmania donovani* has established that the enzyme is not essential for purine salvage in this intracellular protozoan parasite (*7*). Adenine is present at low concentrations in the serum and the cells of mammals, and hypoxanthine is a more abundant precursor for the purine salvage pathways (*2*). The human genetic deficiency of APRTase results in adenine oxidation by xanthine oxidase to 2,8-dihydroxyadenine, a compound with limited solubility, leading to urolithiasis and kidney failure (*8*). Human APRTase deficiency has symptoms with variable-onset and is believed to be reversible upon removal of 2,8-dihydroxyadenine (*8*).

The only structural information on APRTase was reported by Philips et al., using the enzyme from *L. donovani* in complexes with adenine, AMP, and citrate-sulfate ions (*9*). Sequence comparisons indicate that the *L. donovani* enzyme differs from other APRTases by possessing N- and C-terminal extensions that total over 50 amino acids in the overall sequence relative to the structures of *Escherichia coli*, *Saccharomyces cerevisiae*, or human enzymes. Thus, *L. donovani* expresses long-APRTases, while *E. coli*, *S. cerevisiae*, and humans express short-APRTases. This difference is reflected in amino acid sequence conservation, with yeast

[†] Supported by research grant GM41916 from the National Institutes of Health.

[‡] Coordinates for the X-ray crystal structures described here have been deposited at the RCSB structural database as file names 1G2P and 1G2Q.

* Corresponding Author. Telephone: (718) 430-2813. Fax: (718) 430-8565. E-mail: vern@aecom.yu.edu.

[#] These authors contributed equally to this work.

[⊥] Albert Einstein College of Medicine.

[§] Indiana University.

[1] Abbreviations: AMP, adenosine monophosphate; APRTase, adenine phosphoribosyltransferase; HGPRTase, hypoxanthine-guanine phosphoribosyltransferase; HGXPRTase, hypoxanthine-guanine-xanthine phosphoribosyltransferase; immucillinAP, (1*S*)-1-(deazaadenin-9-yl)-1,4-dideoxy-1,4-imino-D-ribitol-5-phosphate; IMP, inosine monophosphate; PRPP, 5-phospho-α-D-ribosyl-1-pyrophosphate; OPRTase, orotate phosphoribosyltransferase.

10.1021/bi010465h CCC: $20.00
Published on Web 08/15/2001

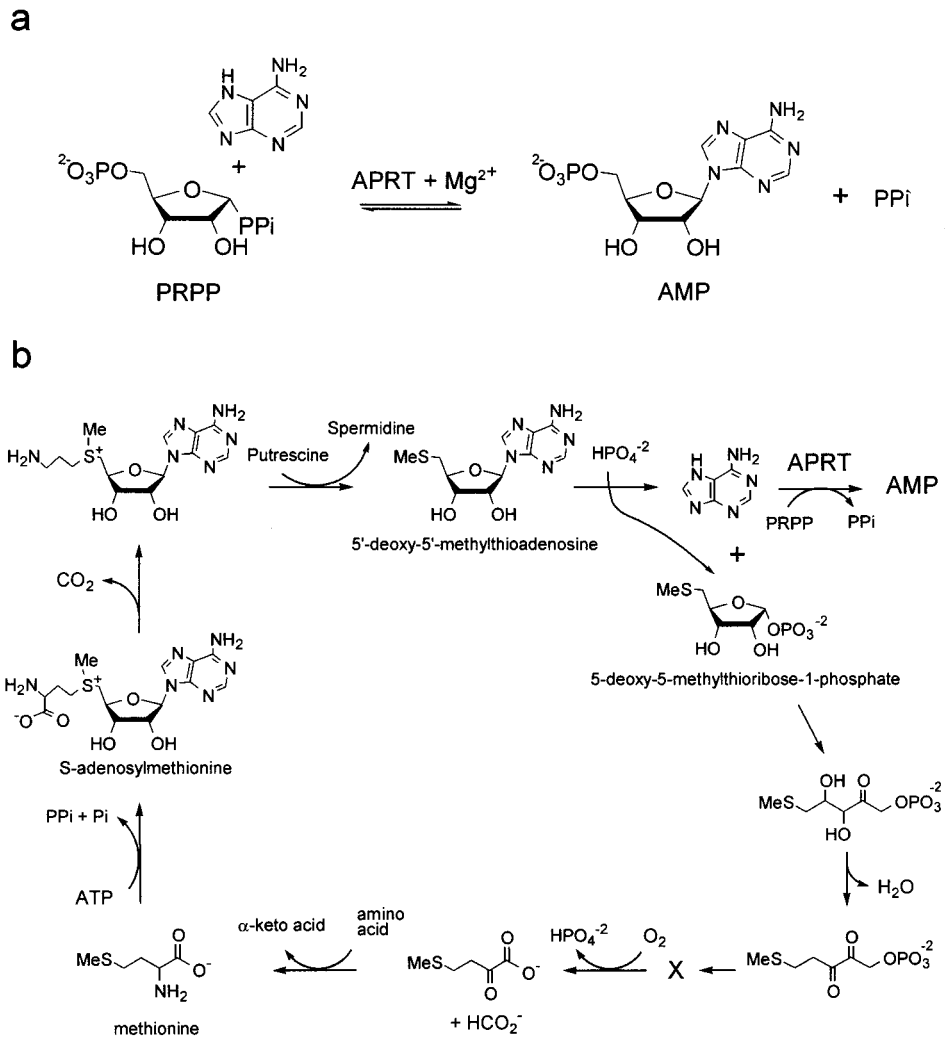

FIGURE 1: Reaction catalyzed by APRTase and its role in *S*-adenosylmethionine metabolism. Mg^{2+}-dependent phosphoribosyl transfer reaction catalyzed by APRTase (a) and salvage pathways for adenine and methionine in the synthesis of spermidine from putrescine and *S*-adenosylmethionine (b).

and human enzymes sharing 29.4 and 29.9% identity with the *Leishmania* enzyme (*9*), while the *E. coli* and yeast enzymes share 40.8 and 41.3% identity with human enzyme, respectively (*10*, *11*). A goal of this work was to characterize the crystal structure of APRTase from *S. cerevisiae* as a representative of the short-APRTases.

MATERIALS AND METHODS

Expression and Purification. The coding sequence of *S. cerevisiae* APRTase cloned into an *N*-terminal 6× His-tagged expression vector (pQE) was used to produce the His-tagged enzyme (*12*). *E. coli* (B25) cells carrying the expression vector were grown at 37 °C in LB containing kanamycin (25 μg/mL), ampicillin (100 μg/mL), and 10 mM sodium phosphate (pH 7.5). Cultures with an A_{260} of 0.7 were induced with 2 mM isopropyl α-D-thiogalactopyranoside and grown for 5 h at 37 °C.

Cells were harvested by centrifugation at 5000*g* for 20 min at 4 °C, suspended in buffer A [50 mM Tris (pH 7.4), 20 mM KCl, 5 mM $MgCl_2$], and disrupted using a French pressure cell. The following steps were carried out at 4 °C with centrifugations at 20000*g* for 20 min. Streptomycin sulfate was added to a final concentration of 1% followed by centrifugation. The supernatant was fractionated by ammonium sulfate precipitation to obtain the fraction between 35 and 70% saturation. The resulting pellet was dialyzed against buffer A containing 50 mM imidazole and loaded onto a 10 mL Ni^{2+} nitrilotriacetic acid (NTA) column (Qiagen). After washing the column with 100 mL of buffer A containing 50 mM imidazole, the protein was eluted with 50 mL of buffer A containing 300 mM imidazole. The fractions with the highest specific activity were combined, concentrated, and dialyzed against buffer A. The enzyme was further purified by Q-Sepharose ion-exchange chromatography with a linear elution gradient of 20−500 mM KCl. The active fractions were combined, concentrated, and dialyzed against buffer A. Purified enzyme was estimated to be greater than 95% homogeneous by analysis on denaturing polyacrylamide gel electrophoresis.

Production of Mutant APRTases. The pQE32-APT1 plasmid was used as the template for all in vitro mutagenic reactions (*12*). The construct contains an N-terminal 6× His tag for easy purification. Mutants were created using the QuickChange method (Stratagene, CA). For mutants that required more than three nucleotide changes, three cycles were added in which the annealing temperature was changed

Table 1: List of Primers Used for the Mutational Studies

mutant	primer (5′ to 3′)
R69A	TATATCGTCGGGTTGGAATCAGCTGGGTTCTTGTTCGGACCA[a,c]
	TGGTCCGAACAAGAACCCAGCTGATTCCAACCCGACGATATA[b,c]
R89A	GGTGTTGGTTTCGTTCCAGTCGCGAAGGCACGTAAGCTACCT[a,d]
	AGGTAGCTTACCTGCCTTCGCGACTGGAACGAAACCAACACC[b,d]
K90A	GTTGGTTTCGTTCCAGTCAGGGCGGCAGGTAAGCTACCTGGC[a,e]
	GCCAGGTAGCTTACCTGCCGCCCTGACTGGAACGAAACCAAC[b,e]
K93A	CTTAAAACATTCGCCAGGTAGAGCTCCTGCCTTCCTGACTGGAAC[a]
	CTTCCAGTCAGGAAGGCAGGAGCTCTACCTGGCGAATGTTTTAAG[b]
Y103F	GAATGTTTTAAGGCTACGTCGAAAAGGAGTACGGT[a]
	ACCGTACTCCTTTTCGAACGTAGCCTTAAAACATTC[b]
E106L	TTTAAGGCTACGTACGAAAAGCTGTACGGTTCTGATCTTTTT[a]
	AAAAAGATCAGAACCGTACAGCTTTTCGTACGTAGCCTTAAA[b]
E106Q	AAGGCTACGTACGAAAAGCAGTACGGTTCTGATCTT[a]
	AAGATCAGAACCGTACTGCTTTTCGTACGTAGCCTT[b]
Y107D	TTTAAGGCTACGTACGAAAAGGAGGACGGTTCTGATCTTTTT[a]
	AAAAAGATCAGAACCGTCCTCCTTTTCGTACGTAGCCTTAAA[b]
Y107F	GCTACGTACGAAAAGGAATTCGGTTCTGATCTTTTT[a]
	AAAAAGATCAGAACCGAATTCCTTTTCGTACGTAGC[b]
G108H	AAGGCTACGTACGAAAAGGAGTACCATTCTGATCTTTTTGAG[a]
	CTCAAAAAGATCAGAATCGTACTCCTTTTCGTACGTAGCCTT[b]
G108A	ACGTACGAAAAGGAGTACGCTTCTGATCTTTTTGAG[a]
	CTCAAAAAGATCAGAAGCGTACTCCTTTTCGTACGT[b]

[a] Upper oligo. [b] Lower oligo. [c] These primers contained a *Pvu* II site. [d] These primers contained an *Nru* I site. [e] These primers contain a *Sac* I site.

from 55 to 50 °C. The oligos for the site-directed mutagenesis are listed in Table 1. Oligonucleotide sequencing confirmed the nucleotide substitutions for each change.

Purification of APRTase mutants was performed according to the Qiagen method except as follows: Cell-free extracts were mixed with 2 mL of Qiagen NTA-nickel beads preequilibrated with lysis buffer and mixed gently for 1 h at 4 °C. The beads were spun down gently, resuspended with 10 mL of lysis buffer, and loaded onto a Poly-Prep chromatography column (BioRad, USA). The column was washed with 20−30 mL of buffer B (50 mM NaH_2PO_4 pH 8.0, 300 mM NaCl, 20 mM imidazole), and the protein was eluted with 10 mL of buffer B containing 250 mM imidazole. The fractions containing APRTase were dialyzed against buffer A containing 20 mM KCl. The protein was analyzed by SDS−PAGE with Coomassie staining, and the total protein concentration was estimated by Bradford assay. The mutant proteins were greater than 95% pure as estimated by denaturing polyacrylamide gel electrophoresis.

Analysis of Kinetic Constants. Reaction mixtures to determine the apparent K_m for adenine contained 50 mM Tris (pH 7.4), 5 mM $MgCl_2$, 0.5 mg/mL bovine serum albumin, 1 mM PRPP, and up to 20 μM adenine. Reaction mixtures to determine the apparent K_m for PRPP contained 250 μM adenine and up to 25 μM PRPP. Reactions were carried out at 37 °C for 5 or 10 min, depending on the extent of the reaction. Product formation was measured as previously reported (*13*). Apparent K_m and k_{cat} values were determined by Lineweaver−Burk plots, fit to the data using the Cricket Graph III program. Each assay was conducted in triplicate, and each kinetic experiment was repeated three times. The reported values are the average of all three experiments. Standard errors of the kinetic constants were less than 25% of the reported values and are not recorded in Table 3.

Crystallization. An orthorhombic crystal form was obtained by mixing 2 μL of 13−15 mg/mL protein with an equal volume of mother liquid containing 100 mM Hepes (pH 7.5) and 1.5 M lithium sulfate, followed by equilibration against 1.0 mL of the mother liquid at 18 °C. Single crystals appeared in 3 days and grew to a maximum size of 0.3 × 0.3 × 0.1 mm^3. These crystals exhibited diffraction consistent with the space group $I2_12_12_1$ with $a = 49.4$ Å, $b = 96.7$ Å, and $c = 112.1$ Å. The crystals contain one subunit in the asymmetric unit with a $V_m = 3.19$ Å^3/Da and a calculated solvent content of 61%. APRTase crystals with an empty catalytic site were obtained using a crystallization buffer containing 100 mM sodium citrate (pH 5.5), 0.2 M sodium acetate, and 20% of poly(ethylene glycol) 5000 monomethyl ether. These crystals exhibited diffraction consistent with the space group P1 with $a = 42.7$ Å, $b = 45.8$ Å, $c = 53.9$ Å, $\alpha = 95.7°$, $\beta = 108.4°$, and $\gamma = 109.6°$. The crystals contain a dimer in the asymmetric unit with a $V_m = 2.18$ Å^3/Da and a calculated solvent content of 43%. Both crystal forms were obtained in the presence of 1.5 mM sodium pyrophosphate, 5 mM $MgCl_2$, 10 mM KCl, and a 1:1.2 molar ratio of immucillinAP,[1] an inhibitor of the enzyme with a K_i of 200 nM.[2] Neither crystal form showed the presence of this inhibitor or MgPPi at the active sites.

Data collection and processing. X-ray diffraction data were collected at −178 °C from single crystals of APRTase using 0.98 Å irradiation and a Quantum CCD detector at beam line X9B (NSLS, Brookhaven National Light Source). Indexing, integration, and scaling of the data were performed with the HKL package (*14*). The data set for the orthorhombic crystal form used for molecular replacement had an overall completeness of 95.5% to 1.75 Å resolution with an R_{sym} of 4.1%. The data set from the triclinic crystal form was 95.8% complete to 1.5 Å resolution with an R_{sym} of 2.4%. Data collection statistics are shown in Table 2.

Molecular Replacement and Structural Refinement. The sulfate form of the orthorhombic crystal form of *S. cerevisiae* APRTase was solved by molecular replacement with AmoRe

[2] Unpublished observations of K. S. E. Tanaka and V. L. Schramm.

Table 2: Data Collection and Refinement Statistics

	apo form	SO_4 form
Diffraction Data		
space group	$P1$	$I2_12_12_1$
resolution range (Å)	20−1.5 (1.55−1.50)[a]	20−1.75 (1.78−1.75)
completeness (%)	95.8 (89.9)	95.5 (82.8)
R_{sym} (%)	2.4 (17.6)	4.1 (24.0)
$I/\sigma I$	28.2 (3.9)	24.0 (2.6)
no. of reflections		
total	132 505	103 449
unique	54 848	26 348
Structure Refinement		
R_{cryst} (%)	19.9	20.8
R_{free} (%)	22.5	23.0
no. of amino acids	356	170
no. of solvent molecules	305	108
no. of ligands		2 SO_4^{2-}
ave protein B-factor (Å^2)	17.9	28.2
ave solvent B-factor (Å^2)	28.6	37.9
ave ligand B-factor (Å^2)		39.9
RMS Deviations from Ideal		
bond (Å)	0.006	0.008
angle (°)	1.345	1.433

[a] Values in parentheses are for the highest-resolution shell.

implemented in CCP4 (*15*) using the *L. donovani* APRTase subunit as the search model (*9*). All nonidentical side chains were trimmed to alanine. A single solution with correlation coefficient of 23.5 and R-factor of 54.2% was generated using 8.0−4.0 Å data from the orthorhombic crystal form. Using XPLOR version 3.851 (*16*), the crystallographic R-factor and free R-factor were reduced to 52.6 and 53.8%, respectively, after 100 steps of rigid-body refinement using 8.0−4.0 Å data. Program O (*17*) was used to view the structure and build the missing side chains into the electron densities in the $2F_o - F_c$ map. The final structure contains residues 4−104 and 109−178, two sulfate ions, and a total of 108 solvent molecules with R_{cryst} of 20.8% and R_{free} of 23.0%.

The yeast APRTase apo structure was solved by molecular replacement using the structure of the sulfate crystal form as the model. The refinement was carried out to 1.5 Å resolution with R_{cryst} and R_{free} values of 19.9 and 22.5%, respectively, using the program CNS (*18*). The final model includes residues 1−178 for each subunit of the dimer in the asymmetric unit and a total of 305 solvent molecules. Both structures show excellent geometry with 99% of the residues in the most favored and additionally allowed region of the Ramachandran plot as evaluated by PROCHECK (*19*). Statistics for the refinement are summarized in Table 2.

RESULTS AND DISCUSSION

Overall Fold. The *S. cerevisiae* APRTase subunit is a single domain structure composed of five α-helices and nine *β*-strands (Figure 2a). This domain can be further divided into the hood (residues 1−35) and the core (residues 36−178) subdomains. The core subdomain consists of a 5-stranded parallel *β*-sheet (*β*3, 61−67; *β*4, 83−90; *β*7, 123−132; *β*8, 150−161 and *β*9, 173−178) and three α-helices (α3, 37−54; α4, 69−81; and α5, 136−148). In the yeast

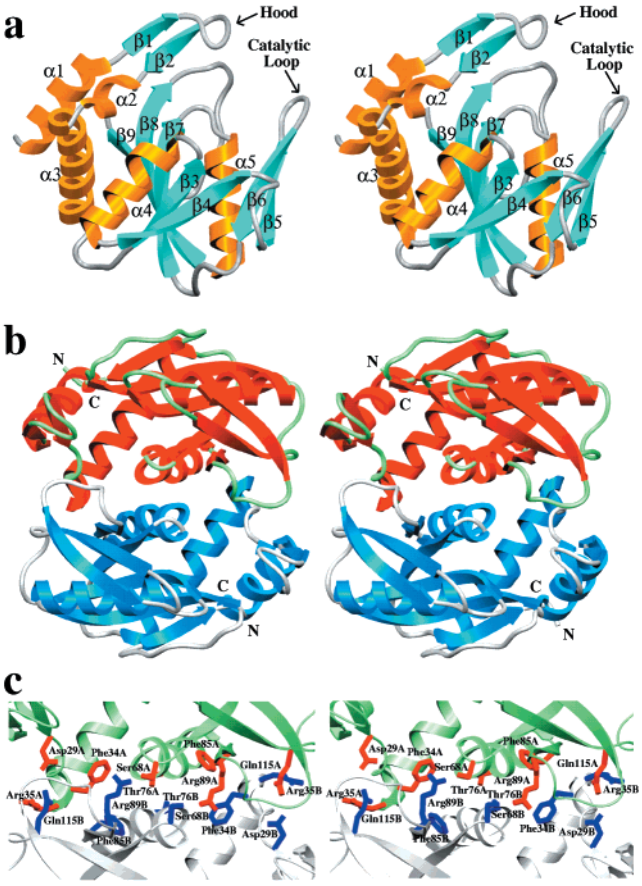

FIGURE 2: Overall structure of yeast APRTase subunit, dimer, and interactions at the dimer interface. Stereoview of yeast APRTase subunit (a), dimer (b), and dimer interface (c). The APRTase consists of five α-helices and nine *β*-strands. In panel b, subunits A and B are depicted in red/green and blue/gray, respectively. The yeast APRTase forms an extensive dimer interface in the crystal structures and involves eight direct hydrogen bonds shown in panel c. Figures 2−4 and 6 were generated using SETOR (*29*).

APRTase apo-enzyme structure the catalytic loop is open, stabilized by crystal packing interactions and reveals a fully defined structure. The hood subdomain of the yeast APRTase is smaller than those found in other type I PRTases and is composed of two *β*-strands and two α-helices (*β*1, 14−18; *β*2, 25−29; α1, 2−13; and α2, 33−35). The segment consisting of residues 97−115, including *β*5 (97−104) and *β*6 (109−115), is referred to as the catalytic loop, and its closure over the active site is thought to be an essential feature of the catalytic mechanism in related PRTases (*20*, *21*). The catalytic sites in both crystal forms contained no detectable nucleotide inhibitor, despite being cocrystallized in the presence of magnesium ion, pyrophosphate, and immucillinAP, a 200 nM inhibitor.[2] The high lithium sulfate and citrate concentrations required for crystallization likely precluded occupancy of the catalytic site. Crystal soakings with immucillinAP and MgPPi in a variety of conditions failed to fill the catalytic site.

Quaternary Structure. The two independent crystal forms show yeast APRTase to be a homodimer (Figure 2b). In the apo-enzyme crystal form, there is a dimer in the asymmetric unit, and the two molecules are similar to each other with a RMS deviation of 0.3 Å for all Cα atoms. In the sulfate bound form, only one subunit is found in the asymmetric unit applying crystallographic symmetry. The dimer interface

is extensive and buries a total surface area of 1400 and 1554 Å^2 on each subunit for the apo-enzyme form and the sulfate bound form, respectively. Despite these extensive contacts, the buried surface area at the dimer interface in yeast APRTase is approximately half of that observed in *L. donovani* APRTase, which buries 2670 Å^2 solvent-accessible surface area for each subunit (*9*). The *L. donovani* enzyme has a 33-amino acid C-terminal extension that wraps around the adjacent subunit, resulting in an unusual large interface area. The dimer interface of *S. cerevisiae* APRTase includes β1-β2, α2-α3, and α4 of one molecule with β4 and α4 of the other molecule. These interactions consist of both hydrogen bond and van der Waals interactions. A total of eight hydrogen bonds are located at the dimer interface including Asp29A OD2-NE2 Gln115B; Phe34A O-N Phe85B; Arg35A NH2-OE1 Gln115B; Ser68A OG-NH2 Arg89B; Thr76A OG1-OG1 Thr76B; Phe85A N-O Phe34B; Gln115A OE1-NH2 Arg35B; and Gln115A NE2-OD2 Asp29B (Figure 2c). Asp29 and Arg89 are completely conserved throughout the short-APRTases.

Sulfate Ion Binding. Crystallization of the orthorhombic crystal form occurred in the presence of 1.5 M Li_2SO_4, resulting in two sulfate ions being located in the active site of APRTase. On the basis of the catalytic site of *L. donovani* APRTase, one sulfate ion is bound at the site typically occupied by the 5′-phosphate portion of the product AMP (Figure 3a,c). This sulfate ion is located in the turn formed by residues 133-Ala−Thr−Gly−Gly−Ser-137. The peptide backbone amide groups of these residues orient toward the bound sulfate and contribute four direct hydrogen bonds. The side chains of Thr134 and Ser137 provide two additional hydrogen bonds to the sulfate ion. Two water molecules are in hydrogen bonding distance (2.7 and 2.8 Å) to this sulfate ion. All five of the amino acids in the Ala133−Ser137 phosphate binding turn are either invariant or highly conserved within the short-APRTases (Figures 5 and 6). This conservation reflects the requirement of a 5′-phosphate for substrate activity in phosphoribosyltransferases and the placement of the 5′-hydroxyl oxygen atom for stabilization of the ribooxocarbenium ion-like transition state proposed for human HGPRTase and demonstrated for purine nucleoside phosphorylase (*20*−*23*). Conservation of this 5′-phosphate binding loop in APRTases supports a similar critical role for 5′-phosphate binding in this enzyme.

The second sulfate ion present in the active site is located at a position proposed for the binding of the β-phosphoryl group of pyrophosphate (Figure 3b,c). This sulfate ion forms a direct hydrogen bond with the main chain amide of Ser68. In both apo and sulfate bound forms of yeast APRTase, residues Glu67−Ser68 form a nonproline cis peptide linkage that orients the amide group of Ser68 toward the sulfate ion. A hydrogen bond between the side chains of Arg89 and Ser68 at the dimer interface stabilizes the cis peptide bond geometry to permit this interaction (Figure 2c). Arg89 is completely conserved in short-APRTases, but either Ser or Ala is found at position 68. A similar cis peptide conformation has been observed at the corresponding position in other type I PRTases, including human and malarial HGXPRTases in complex with transition state inhibitors (*20*, *21*). Since backbone contacts to the catalytic sites are involved, the amino acid residues involved in cis peptide formation are not conserved. In contrast, the side chain of Arg69 is located

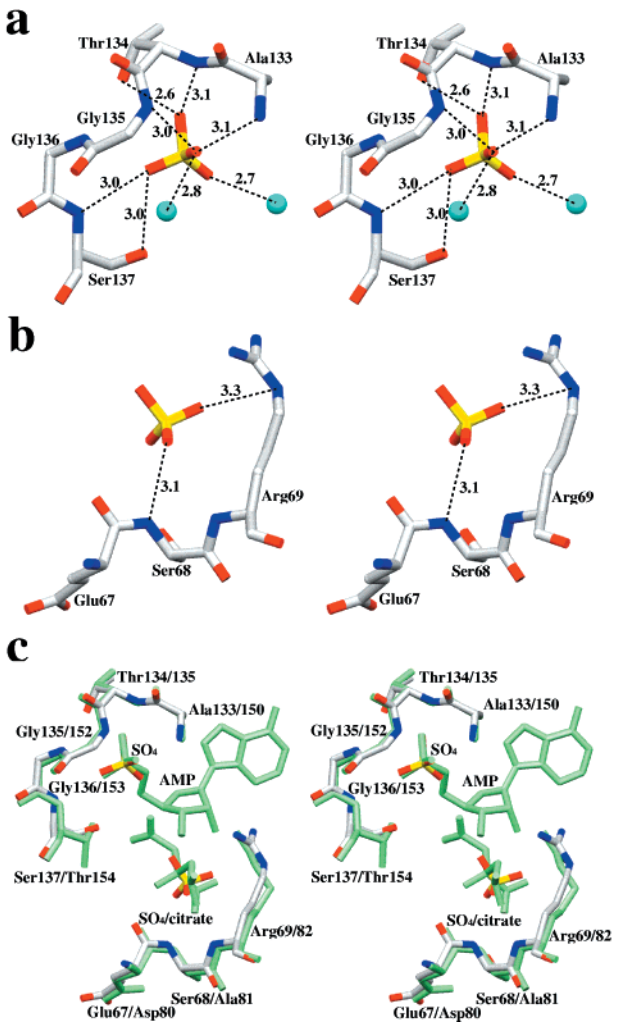

FIGURE 3: Two sulfate binding sites in yeast APRTase and comparison to components at the *L. donovani* APRTase active site. Stereoview of the sulfate binding site in yeast APRTase coincident with the 5′-phosphate site of AMP in the *L. donovani* APRTase (a). A stereoview of the sulfate binding site corresponding to the citrate binding site in *L. donovani* APRTase, proposed to be the α-pyrophosphoryl binding site of PRPP (b). Yeast APRTase and sulfate binding sites (green) are compared with the AMP/citrate binding sites from *L. donovani* APRTase shown with gray carbons and colored heteroatoms (c). The location of AMP and surrounding protein is taken from ref *9*.

near the sulfate ion contributing a 3.3 Å hydrogen bond. Arg69 is absolutely conserved in APRTases indicating an essential interaction with the pyrophosphate group for catalytic function (see below). Both sulfate ions in yeast APRTase structure bind at similar positions as the two sulfate ions observed in the sulfate bound form of *L. donovani* APRTase (*9*).

Structural Comparison. The yeast APRTase apo-enzyme and sulfate-bound crystal forms were solved to 1.5 and 1.75 Å, respectively. The two structures are similar with RMS deviations of 1.1 Å for all Cα atoms. The overlap of Cα traces for the two structures reveals differences in two flexible loops. These are residues 15−29 (loop I) in the hood subdomain and residues 159−172 (loop II) in the core subdomain (Figure 4a). Both loops are in the vicinity of the active site, although they are not directly involved in binding the sulfate ions. Phe27 from loop I in the hood subdomain is a highly conserved residue in close van der Waals contact

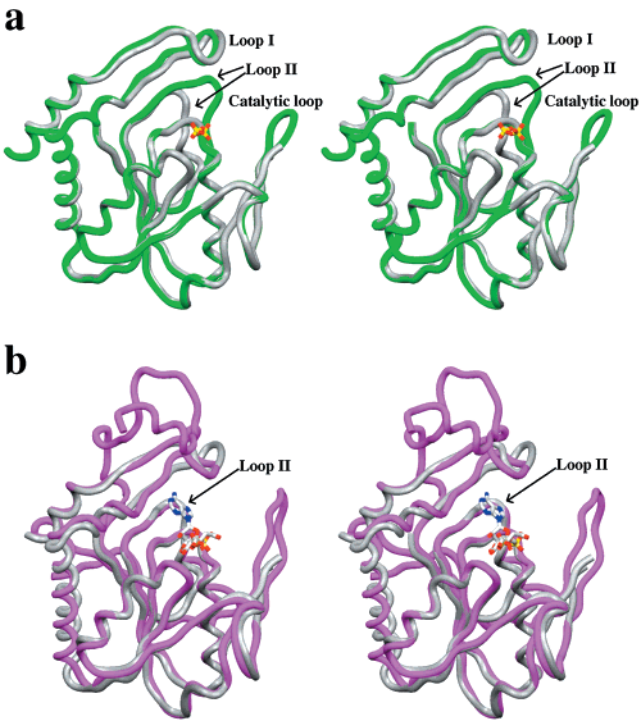

FIGURE 4: Peptide backbone diagrams comparing sulfate-bound yeast APRTase with the apo-enzyme structure and with the *L. donovani* APRTase structure. Superposition of yeast APRTase apo-enzyme (green) with sulfate-bound (gray) structure (a). Superposition of yeast APRTase sulfate-bound structure (gray) with *L. donovani* APRTase ternary complex with AMP and citrate (magenta) in panel b. Loop I (residues 15−29), loop II (residues 159−172), and the catalytic loop (residues 99−115) are labeled in panel a. Loop II regions in yeast APRTase sulfate-bound structure and *Leishmania* APRTase ternary complex demonstrate similar conformations despite lack of sequence homology, shown in panel b.

to Arg69, which interacts with the second bound sulfate ion. Loop I in the sulfate-bound structure moves approximately 1.0−1.5 Å closer to the active site. Loop II residues 159−172 interact with residues in the 5′-phosphate binding loop, mostly through backbone atoms. Upon binding of the two sulfate ions, loop II demonstrates a large change in structure that is not related to crystal packing. In the sulfate-bound form, residues 162−164 moved approximately 5−7 Å closer to the core of structure. None of the amino acid side chains in loop II are in contact with substrate or the phosphate-binding loop. Accordingly, none of the amino acids of loop II are completely conserved in the APRTase enzymes (Figure 5).

Contacts between loop II and the residues in the active site are more extensive in the apo-enzyme structure than the sulfate-bound complex. Four hydrogen bonds between the 5′-phosphate binding loop and loop II in the apo-enzyme include the carbonyl oxygen of Met159 with the amide group of Ile132, the amide group of Leu161 with the carbonyl oxygen of Asp130, the amide group of Ser168 with the carbonyl oxygen of Thr134 and the side chain OG of Ser168 with the carbonyl oxygen of Gly135. In the sulfate-bound yeast APRTase structure, only the first two hydrogen bonds are observed. The high conservation of the amino acids Phe27 and 133-Ala−Thr−Gly−Gly−Ser-137 supports an essential role for both loops I and II in APRTase catalysis.

Amino acids in the catalytic loop (β5−β6, residues 99−115, Figure 2a) of the apo-enzyme structure are completely ordered as a consequence of crystal contacts between this loop and a symmetry-related molecule. This interaction accounts for the rare observation of an open and ordered catalytic loop. In most loop-open structures of phosphoribosyltransferases, these residues are disordered (for example see ref *24*). In the structure with bound sulfate, the loop is not stabilized by crystal packing contacts. As a consequence, four residues at the tip of the catalytic loop are disordered and are not included in the final refined structure. The catalytic loops in both structures are in the open conformation and neither displays the translocation over the catalytic site known to occur in purine PRTases with bound transition state analogue inhibitors (*20*, *21*).

Comparison of Short- and Long-APRTases. The *S. cerevisiae* and *L. donovani* APRTases share less than 30% sequence identity. The structural differences result in a RMS deviation of 2.2 Å for a total of 172 Cα atoms when the yeast APRTase apo-enzyme is compared to the *L. donovani* APRTase complex with AMP and citrate. The greatest difference is in the C-terminal extension of *L. donovani* APRTase that extends and coils around the adjacent subunit in the dimeric structure (Figure 4b). Yeast APRTase is missing these 33 residues but still forms an extensive dimer interface, similar to that observed in the *L. donovani* APRTase structure (Figure 2b,c).

Other differences between the yeast and *L. donovani* APRTases occur in the three flexible loop regions; the hood (15−29), catalytic loop (99−115), and loop II (159−172). The catalytic loop in the *L. donovani* enzyme is four residues longer and is in an open conformation similar to that observed in the yeast APRTase structures (*9*). The primary sequence of this region in the *L. donovani* enzyme corresponds to residues 159−172 in the yeast enzyme but has multiple amino acid insertions. This segment in *L. donovani* APRTase consists of a loop−turn−loop structure followed by a short helix. Similar structural features are observed in yeast APRTase upon the binding of the sulfate ions although the loop-turn-loop structure is nine residues shorter (Figure 4b). However, in the yeast APRTase apo-enzyme structure, this segment folds into a completely ordered loop.

Comparison of APRTase with OPRTase. Orotate phosphoribosyltransferase (OPRTase) is the closest structural member to APRTase within the type I PRTase family. Yeast APRTase shares 23% sequence identity with *Salmonella typhimurium* OPRTase, while it has no apparent sequence homology with other purine phosphoribosyltransferases, such as the HGXPRTase from malaria. The core structures of APRTase and OPRTase are similar, with an RMS deviation of 3.4 Å between yeast APRTase and *S. typhimurium* OPRTase for 155 Cα atoms (*24*). The main differences are located in the hood region, since APRTase has a much smaller hood, and also at the catalytic loop region. Yeast APRTase and *S. typhimurium* OPRTase form similar dimer interfaces, and both of these differ from those observed in other members from the type I PRTase family. However, the catalytic loop in *S. typhimurium* OPRTase is located near the dimer interface and is believed to close onto the active site of the opposite subunit. In contrast, the catalytic loop in yeast APRTase extends away from the dimer interface and closes onto the active site of the same subunit.

Correlation of Conserved Amino Acids with APRTase Structure. Genomic databases report 33 amino acid se-

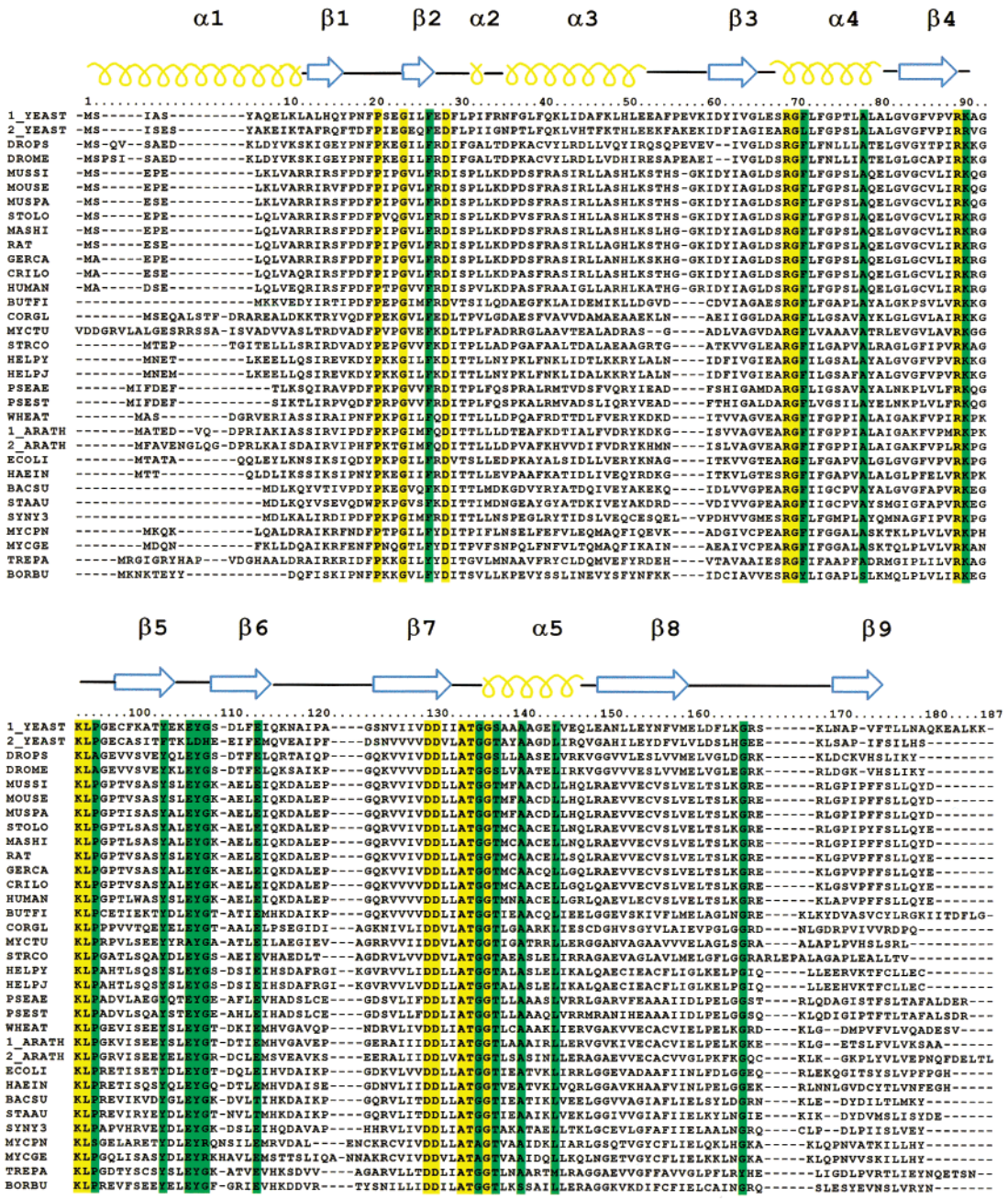

FIGURE 5: Sequence alignment of APRTases from 33 species using the ClustalX software package (*25*). The 13 residues that are conserved in all APRTases are colored in gold. Those sequences conserved in 30 or more of the 33 APRTases are colored in green. Structure of the protein is indicated above the sequences, with yellow coils, arrows, and lines representing α-helices, *β*-sheets, and connecting loops or unstructured elements, respectively. 1_yeast and 2_yeast-*Saccharomyces cerevisiae*; drops-*Drosophila pseudoobscura*; drome-*Drosophila melanogaster*; mussi-*Mus spicilegus*; mouse-*Mus musculus*; muspa-*Mus pahari*; stolo-*Stochomys longicaudatus*; mashi-*Mastomys hildebrandtii*; rat-*Rattus norvegicus*; gerca-*Gerbillus campestris*; crilo-*Cricetulus longicaudatus*; human-*Homo sapiens*; butfi-*Butyrivibrio fibrisolvens*; corgl-*Corynebacterium glutamicum*; myctu-*Mycobacterium tuberculosis*; strco-*Streptomyces coelicolor*; helpy-*Helicobacter pylori*; helpj-*Helicobacter pylori J99*; pseae-*Pseudomonas aeruginosa*; psest-*Pseudomonas stutzeri*; wheat-*Triticum asetivum*; 1_arath and 2_arath-*Arabidopsis thaliana*; ecoli-*Escherichia coli*; haein-*Haemophilus influenzae*; bacsu-*Bacillus subtilis*; staau-*Staphylococcus aureus*; syny3-*Synechocystis PCC6803*; mycpn-*Mycoplasma pneumoniae*; mycge-*Mycoplasma genitalium*; trepa-*Treponema pallidum*; borbu-*Borrelia burgdorferi*.

quences[3] that align with sufficient homology to be identified as short-APRTases, (Figure 5) (*25*). Only 13 invariant amino acid residues (yellow in Figure 5) are observed in the approximately 180 amino acids of these enzymes. Another 15 residues are conserved in 30 or more of the 33 APRTase sequences (green). Structural alignment of these residues is indicated in Figure 6. The structurally conserved α-helix and *β*-sheet that defines the core of type I PRTases does not show significant amino acid conservation. The highly conserved residues cluster in the catalytic site, the hinge, and the tip regions of the catalytic loop and hood regions (loop I) of the catalytic site (Figure 6). In related PRTases, residues corresponding to 133-Ala−Thr−Gly−Gly−Ser-137 are defined as the 5′-phosphate binding loop, 69-Arg−Gly−Phe-

[3] The database search was conducted in January 2001.

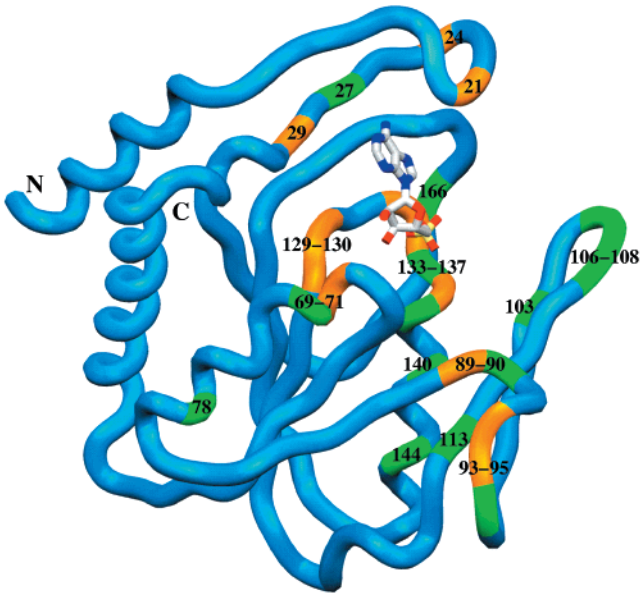

FIGURE 6: Yeast APRTase backbone structure showing the positions of the 13 amino acids conserved in all APRTases (yellow) and the residues conserved in 30 or more of the 33 APRTases (green). The location of AMP was assumed from the *L. donovani* structure (*9*).

71 are involved in Mg-pyrophosphate binding, and Asp129 and Asp130 share hydrogen bonds with the 2′- and 3′-hydroxyls to IMP or other nucleotide monophosphates and interact with Mg^{2+}. Arg89 and Lys90 are adjacent to the cis peptide bond between residues Glu67−Ser68, which are in contact with pyrophosphate. Tyr103 and 106-Glu−Tyr−Gly-108 are located in the catalytic loop that is proposed to close over the active site during catalysis. The hinge region to the catalytic loop (residues 99−115) is formed by residues 93-Lys−Leu−Pro-95. Catalytic site interactions in PRTase extend beyond the first sphere of amino acids and the conservation of the second sphere amino acids indicates that loop 91−96 is required for transmitting essential conformational changes to the catalytic site. Pro21, Gly24, Phe27, and Asp29 are highly conserved in the hood region (loop I) that is proposed to close over the purine ring during catalysis. Yeast APRTase differs considerably from the well-characterized HGXPRTases in this region, with the hood being composed of C-terminal residues (β1−loop−β2) rather than the N-terminal region (β9−loop−β10). Adenine base activation is required for catalysis and in other purine PRTases is often achieved by N7 protonation, a proposed role for Asp29, the only conserved carboxylic acid in this loop (*20*, *21*).

Mutagenesis of Conserved Amino Acids. The completely conserved Arg69 is located near the *N*-terminal end of α4, the proposed pyrophosphate binding site of yeast APRTase (Figure 3b). The equivalent amino acid in *L. donovani* APRTase is Arg82. It forms hydrogen bonds from the guanidinium group to citrate bound in the site proposed for pyrophosphate binding, to O2′ of bound AMP and to a water-mediated hydrogen bond with N3 of the purine ring. The backbone amide of Arg82 in *L. donovani* APRTase also interacts with bound citrate (*9*). Although there has been no structure of an APRTase with pyrophosphate bound, this amino acid is a strong candidate for substrate binding and catalytic function. The mutation Arg69Ala decreased the k_{cat} by 4 orders of magnitude with no change in the K_m for PRPP but a 6-fold increase in the K_m for adenine (Table 3). Arg69 is therefore important for transition state stabilization, with relatively small effects on substrate binding. The position of Arg69 in the catalytic site is pertinent to the proposed mechanism of *N*-ribosyl transferases. It is proposed that these enzymes enhance the nucleophilicity of both purine and pyrophosphate groups, promoting the migration of the ribooxocarbenium ion between the nucleophiles fixed at the catalytic site (*21*, *22*). Arg69 in yeast APRTase and other short-APRTases is proposed to accomplish this role by its multiple interactions at the MgPPi binding site.

Table 3: Kinetic Properties of Catalytic Loop Mutants of Yeast APRTase[a]

mutation	k_{cat} (s^{-1})	k_{cat}/K_m (M^{-1}, s^{-1})	$K_{m,app}$ adenine (μM)	$K_{m,app}$ PRPP (μM)
WT	30	3×10^6	9	20
R69A	3×10^{-3}	60	50	20
R89A	10	5×10^5	30	50
K90A	0.8	1×10^5	8	20
K93A	40	2×10^6	20	50
Y103F	100	2×10^6	50	100
E106L[b]	1×10^{-4}	2	60	6
E106Q	5×10^{-2}	6×10^3	9	2
Y107D[b]	0.3	3×10^3	90	20
Y107F	4	2×10^5	30	30
G108H[b]	0.7	3×10^4	20	40
G108A	30	4×10^5	70	50

[a] The k_{cat}, k_{cat}/K_m, and $K_{m,app}$ adenine were determined at a fixed concentration of 1 mM PRPP with varied adenine. This concentration of PRPP is greater than 10 times the apparent K_m for PRPP for all mutants. The $K_{m,app}$ PRPP was determined at a fixed adenine concentration of 250 μM with varied PRPP. [b] These mutations were described earlier (*28*) but were not fully characterized.

Arg89 and Lys90 are near the end of β4, with the side chain of Arg89 pointed toward the adjacent subunit (Figure 2c), and in contact with the side chain of Ser68 from the adjacent subunit. In addition to forming an important contact for the dimer interface, this interaction may stabilizes the cis peptide bond between Glu67−Ser68. The backbone amide at the cis peptide in human and malarial phosphoribosyltransferases is known to form contacts with two oxygen atoms of the MgPPi complex, an interaction possible only with the cis configuration (*20*, *21*). Surprisingly, the Arg89Ala mutation in APRTase causes only minor changes in the K_m for PRPP and decreases k_{cat} only 2-fold (Table 3). Thus, the other interactions that form the dimer interface are sufficient to stabilize the cis peptide, or its presence plays a relatively small role in catalysis. The side chain of the highly conserved adjacent Lys90 is directed toward the pyrophosphate binding site, in hydrophobic contact with Glu67. The mutation Lys90Ala decreased k_{cat} by a factor of approximately 30, with no significant change in substrate K_m values. The mutation of conserved Lys93 to Ala caused small increases in substrate K_m values and also a small increase in k_{cat}, implying an increase in the rate-limiting step of catalysis.

Mutations that increase k_{cat} are rare, but the Tyr103Phe mutation increases k_{cat} by a factor of 4. In the phosphoribosyltransferases, catalysis is usually limited by the rate of product release (*26*). Thus, mutations that permit more facile release of products cause an increase in the k_{cat}. The Tyr103Phe mutant falls into this category, with approximately the same magnitude of increase in the K_m values for adenine and PRPP as the increase in k_{cat} (Table 3). The

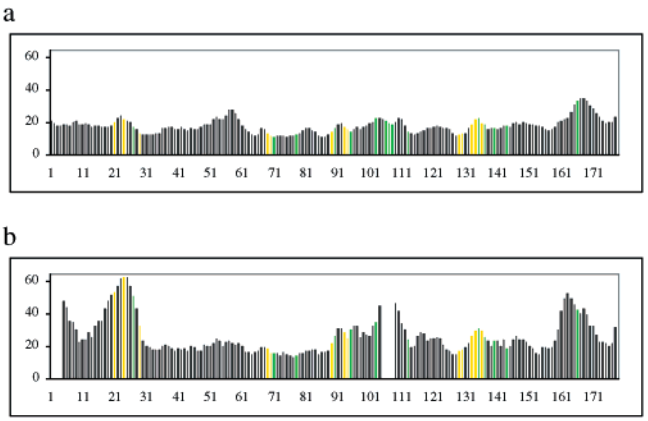

FIGURE 7: Crystallographic B-factors for the yeast APRTase apo-enzyme (a) or with two sulfate ions bound in the catalytic site (b). Note that the conserved residues (yellow and green in panels a and b often correlate with areas of the protein that have increased B-factors. Missing residues (105−108 in b) are located at the tip of the catalytic site loop.

Lys93Ala mutation discussed above, exhibits similar properties. These mutants cause a minimal change in k_{cat}/K_m, since a similar increase occurs in the numerator and denominator. Product release in phosphoribosyltransferases is thought to be governed by the loop motions that accompany catalytic site filling and emptying (*27*). It is significant that Tyr103 is located in a hinge region for the catalytic site loop. The side chain hydroxyl of Tyr103 is pointed toward the active site to form a 2.9 Å hydrogen bond with the side chain of Thr134 in the sulfate-bound structure. With catalysis limited by the rate of loop opening and product release, loss of a hydrogen bond interaction in the Tyr103Phe mutant would increase the rate at which the loop opens and closes, thereby altering the catalytic rate.

Mutations in the tip of the catalytic loop (106−108) identified Glu106Leu to be the most debilitating for catalysis (Table 3). With the loop-open structures reported here, the catalytic role of Glu106 cannot be rigorously assigned. However, in loop-closed purine phosphoribosyltransferases, two residues from the closed catalytic site loop make direct contact to the 5′-phosphate and a pyrophosphate oxygen (*20*, *21*). The mutation Glu106Leu prevents this interaction and decreases k_{cat}/K_m by a factor of approximately one million. In contrast, Glu106Gln is 3 orders of magnitude more active than Glu106Leu, presumably by restoring the ability to hydrogen bond, but in a nonoptimal way. Mutations in the adjacent groups, Tyr107Phe and Gly108Ala, caused relatively small changes in the catalytic properties (Table 3). Replacements Tyr107Asp and Gly108His are more catalytically debilitating, causing 2 to 3 orders of magnitude decrease in k_{cat}/K_m as compared to wild-type enzyme. Although there is significant increase in the K_m for adenine, most of the change is in k_{cat}. These loop mutations could influence catalysis either by slowing loop dynamics and/or by altered interactions with the bound substrate. Future work requires the crystallographic analysis of closed complexes of APRTase with transition state analogues and rates of catalytic site loop motion (measurements by NMR) to resolve these mechanistic questions (*26*).

B-Factor Analysis of Conserved Amino Acids in Yeast APRTase. Conserved regions of yeast APRTase were examined for their crystallographic B-factors (Figure 7). The loop I hood (21−29) forms part of the purine site and shields the site from solvent. In related phosphoribosyltransferases (*20*, *21*), the hood provides chemical activation by increasing the nucleophilicity at N7. The hood demonstrates increased B-factors relative to neighboring residues in both apo-enzyme and the sulfate-bond form (Figure 7a,b). Conserved residues 69−71 form the pyrophosphate binding site and show small B-factors relative to neighboring groups in both enzyme forms. Conserved residues 89 and 90 form a loop involved in stabilizing the pyrophosphate binding site. The three residues at the tip of the major catalytic site loop, 106−108, show weak electron density in the sulfate-bound enzyme structure suggesting disorder (Figure 7b). However, the apo-APRTase has the catalytic site loop stabilized by crystal packing interactions (Figure 7a). Region 129−137 plays a major catalytic role in 5′-phosphate recognition and is the most highly conserved portion of the APRTases. It also coordinates magnesium binding and orientation of the nucleotide through interactions with the 2′- and 3′-hydroxyls. In both structures described here, amino acids 129−137 remain relatively mobile as compared to neighboring groups.

Conserved Amino Acids in Hinge Regions of Yeast APRTase. A surprise from the location of conserved amino acids is that conserved amino acids Ala78, Ala140, Leu144, Gly166, and residues 93−95 play no direct role in catalytic site contacts. These conserved residues are located near hinge regions and may be required to maintain the loop motions essential for catalysis.

SUMMARY AND CONCLUSIONS

Yeast APRTase is a representative member of the short-APRTases found widely distributed in both prokaryotes and eukaryotes. The structure of yeast APRTase demonstrates the canonical α-helix and β-sheet structures of PRTases with truncated catalytic site loops. Only 13 amino acids are absolutely conserved in the APRTases based on genomic analysis. These residues function as hinges to catalytic site loops, as substrate contact residues in these loops and as catalytic site ligands. Conservation of essential residues in APRTases includes elements required for protein motion and for chemical interactions at the catalytic site. Mutations increasing k_{cat} have kinetic and structural properties consistent with altered loop dynamics, while those decreasing k_{cat} alter the interaction to bound substrates.

REFERENCES

1. Flaks, J. G., Erwin, M. J., and Buchanan, J. M. (1957) *J. Biol. Chem. 228*, 201−213.
2. Hammond, D. J., and Gutteridge, W. E. (1984) *Mol. Biochem. Parasitol. 13*, 243−261.
3. Myers, R. W., and Abeles, R. H. (1989) *J. Biol. Chem. 264*, 10547−10551.
4. Myers, R. W., Wray, J. W., Fish, S., and Abeles, R. H. (1993) *J. Biol. Chem. 268*, 24785−24791.
5. Berens, R. L., Krug, E. C., and Marr, J. J. (1995) in *Biochemistry and Molecular Biology of Parasites* (Marr, J. J., and Müller, M., Eds.) pp 89−117, Academic Press Limited, London.
6. Dai, Y., Pochapsky, T. C., and Abeles, R. H. (2001) *Biochemistry 40*, 6379−6387.
7. Hwang, H.-Y., and Ullman, B. (1997) *J. Biol. Chem. 272*, 19488−19496.
8. Simmonds, H. A., Sahota, A. S., and Van Acker, K. J. (1995) in *The Metabolic and Molecular Bases of Inherited Disease*

(Scriver, C. R., Beaudet, A. L., Sly, W. S., and Valle, D., Eds.) pp 1707−1724, McGraw-Hill, Inc., New York.
9. Phillips, C. L., Ullman, B., Brennan, R. G., and Hill, C. P. (1999) *EMBO J. 18*, 3533−3545.
10. Broderick, T. P., Schaff, D. A., Bertino, A. M., Dush, M. K., Tischfield, J. A., and Stambrook, P. J. (1987) *Proc. Natl. Acad. Sci. U.S.A. 84*, 3349−3353.
11. Alfonzo, J. D., Sahota, A., and Taylor, M. W. (1997) *Biochim. Biophys. Acta 1341*, 173−182.
12. Alfonzo, J. D., Crother, T. R., Guetsova, M. L., Daignan-Fornier, B., and Taylor, M. W. (1999) *J. Bacteriol. 181*, 347−352.
13. Hershey, H. V., and Taylor, M. W. (1978) *Prep. Biochem. 8*, 453−462.
14. Otwinowski, Z., and Minor, W. (1997) *Methods Enzymol. 276*, 307−326.
15. Navaza, J. (1994) *Acta Crystallogr. A50*, 157−163.
16. Brunger, A. T. (1992), Yale University Press, New Haven, Connecticut.
17. Jones, T. A. (1985) *Methods Enzymol. B115*, 157−171.
18. Brunger, A. T., et al. (1998) *Acta Crystallogr. D54*, 905−921.
19. Laskowski, R. A., MacArthur, M. W., Moss, D. S., and Thornton, J. M. (1993) *J. Appl. Crystallogr. 26*, 283−291.
20. Shi, W., Li, C. M., Tyler, P. C., Furneaux, R. H., Grubmeyer, C., Schramm, V. L., and Almo, S. C. (1999) *Nat. Struct. Biol. 6*, 588−593.
21. Shi, W., Li, C. M., Tyler, P. C., Furneaux, R. H., Cahill, S. M., Girvin, M. E., Grubmeyer, C., Schramm, V. L., and Almo, S. C. (1999) *Biochemistry 38*, 9872−9880.
22. Fedorov, A., Shi, W., Kicska, G., Fedorov, E., Tyler, P. C., Furneaux, R. H., Hanson, J. C., Gainsford, G. J., Larese, J. Z., Schramm, V. L., and Almo, S. C. (2001) *Biochemistry 40*, 853−860.
23. Kline, P. C., and Schramm, V. L. (1995) *Biochemistry 34*, 1153−1162.
24. Scapin, G., Ozturk, D. H., Grubmeyer, C., and Sacchettini, J. C. (1995) *Biochemistry 34*, 10744−10754.
25. Thompson, J. D., Gibson, T. J., Plewniak, F., Jeanmougin, F., and Higgins, D. G. (1997) *Nucleic Acid Res. 25*, 4876−4882.
26. Xu, Y., and Grubmeyer, C. (1998) *Biochemistry 37*, 4114−4124.
27. Wang, G., P., Cahill, S. M., Liu, X., Girvin, M. E., and Grubmeyer, C. (1999) *Biochemistry 38*, 284−295.
28. Crother, T. R., and Taylor, M. W. (1998) *Adv. Exp. Med. Biol. 431*, 309−314.
29. Evan, S. V. (1993) *J. Mol. Graphics 11*, 134−138.

BI010465H